Identification of Autoantibodies against TRPM1 in Patients with Paraneoplastic Retinopathy Associated with ON Bipolar Cell Dysfunction

Mineo Kondo[1*☯], Rikako Sanuki[2,3☯], Shinji Ueno[1], Yuji Nishizawa[4], Naozumi Hashimoto[5], Hiroshi Ohguro[6], Shuichi Yamamoto[7], Shigeki Machida[8], Hiroko Terasaki[1], Grazyna Adamus[9], Takahisa Furukawa[2,3*]

1 Department of Ophthalmology, Nagoya University Graduate School of Medicine, Nagoya, Aichi, Japan, **2** Department of Developmental Biology, Osaka Bioscience Institute, Suita, Osaka, Japan, **3** JST, CREST, Suita, Osaka, Japan, **4** Department of Biomedical Sciences, Chubu University, Kasugai, Aichi, Japan, **5** Department of Respiratory Medicine, Nagoya University Graduate School of Medicine, Nagoya, Aichi, Japan, **6** Department of Ophthalmology, Sapporo Medical University School of Medicine, Sapporo, Hokkaido, Japan, **7** Department of Ophthalmology and Visual Science, Chiba University Graduate School of Medicine, Chiba, Chiba, Japan, **8** Department of Ophthalmology, Iwate Medical University School of Medicine, Morioka, Iwate, Japan, **9** Department of Ophthalmology, Oregon Health and Science University, Portland, Oregon, United States of America

Abstract

Background: Paraneoplastic retinopathy (PR), including cancer-associated retinopathy (CAR) and melanoma-associated retinopathy (MAR), is a progressive retinal disease caused by antibodies generated against neoplasms not associated with the eye. While several autoantibodies against retinal antigens have been identified, there has been no known autoantibody reacting specifically against bipolar cell antigens in the sera of patients with PR. We previously reported that the transient receptor potential cation channel, subfamily M, member 1 (TRPM1) is specifically expressed in retinal ON bipolar cells and functions as a component of ON bipolar cell transduction channels. In addition, this and other groups have reported that human TRPM1 mutations are associated with the complete form of congenital stationary night blindness. The purpose of the current study is to investigate whether there are autoantibodies against TRPM1 in the sera of PR patients exhibiting ON bipolar cell dysfunction.

Methodology/Principal Findings: We performed Western blot analysis to identify an autoantibody against TRPM1 in the serum of a patient with lung CAR. The electroretinograms of this patient showed a severely reduced ON response with normal OFF response, indicating that the defect is in the signal transmission between photoreceptors and ON bipolar cells. We also investigated the sera of 26 patients with MAR for autoantibodies against TRPM1 because MAR patients are known to exhibit retinal ON bipolar cell dysfunction. Two of the patients were found to have autoantibodies against TRPM1 in their sera.

Conclusion/Significance: Our study reveals TRPM1 to be one of the autoantigens targeted by autoantibodies in at least some patients with CAR or MAR associated with retinal ON bipolar cell dysfunction.

Citation: Kondo M, Sanuki R, Ueno S, Nishizawa Y, Hashimoto N, et al. (2011) Identification of Autoantibodies against TRPM1 in Patients with Paraneoplastic Retinopathy Associated with ON Bipolar Cell Dysfunction. PLoS ONE 6(5): e19911. doi:10.1371/journal.pone.0019911

Editor: Steven Barnes, Dalhousie University, Canada

Received February 10, 2011; **Accepted** April 6, 2011; **Published** May 17, 2011

Funding: This work was supported by CREST from the Japan Science and Technology Agency (http://www.jst.go.jp/), and a Grant-in-Aid for Scientific Research (B)(C) (#20390448, #20390087, #20592075, #20791678) from the Ministry of Education, Culture, Sports, Science and Technology (http://www.jsps.go.jp/), the Takeda Science Foundation (http://www.takeda-sci.or.jp/), The Uehara Memorial Foundation (http://www.ueharazaidan.com/), the Naito Foundation (http://www.naito-f.or.jp/), the Novartis Foundation (#20-10, http://novartisfound.or.jp/), Mochida Memorial Foundation for Medical and Pharmaceutical Research (http://www.mochida.co.jp/zaidan/), the Senri Life Science Foundation (#S-2144, http://www.senri-life.or.jp/), the Kato Memorial Bioscience Foundation (http://www.katokinen.or.jp/) and the Japan National Society for the Prevention of Blindness (http://www.nichigan.or.jp/link/situmei.jsp). A grant from the National Institute of Health (E13053), was awarded to GA. The funders had no role in study design, data collection and analysis, decision to publish, or preparation of the manuscript.

Competing Interests: The authors have declared that no competing interests exist.

* E-mail: furukawa@obi.or.jp (TF); kondomi@med.nagoya-u.ac.jp (MK)

☯ These authors contributed equally to this work.

Introduction

Paraneoplastic retinopathy (PR) is a progressive retinal disorder caused by an autoimmune mechanism and is associated with the presence of anti-retinal antibodies in the serum generated against neoplasms not associated with the eye [1–4]. The retinopathy can develop either before or after the diagnosis of a neoplasm. Patients with PR can have night blindness, photopsia, ring scotoma, attenuated retinal arteriole, and abnormal electroretinograms (ERGs). The diagnosis of PR is usually made by the identification of neoplasms and anti-retinal autoantibodies in the sera.

PR includes two subgroups: cancer-associated retinopathy (CAR) [5,6] and melanoma-associated retinopathy (MAR) [7–10]. Although CAR and MAR share similar clinical symptoms, the ERG findings

are very different. Both a- and b-waves are severely attenuated in CAR, indicating extensive photoreceptor dysfunction, whereas only the b-wave is severely reduced while the a-wave is normal in MAR, suggesting bipolar cell dysfunction [8,9]. However, it was recently reported that cancers other than melanoma can cause bipolar cell dysfunction [11,12]. Several autoantibodies against retinal antigens have been identified, but a specific antigen associated with bipolar cells has not been identified in patients with CAR and MAR [1–10].

In the current study, we identified autoantibodies against the transient receptor potential cation channel, subfamily M, member 1 (TRPM1) [13–15] in the serum of one patient with lung cancer. The ERG findings in this patient indicated a selective ON-bipolar cell dysfunction. We also investigated the sera of 26 MAR patients and found that two contained autoantibodies against TRPM1. Our results suggest that TRPM1 is one of the retinal autoantigens in at least some patients with CAR or MAR and may cause retinal ON bipolar cell dysfunction.

Results

Case report of CAR associated with ON bipolar cell dysfunction

A 69-year-old man visited the Nagoya University Hospital with complaints of blurred vision, photopsia and night blindness in both eyes of three months duration. At this point he was not diagnosed as suffering from any eye disease or systemic disease, including a malignant tumor, and his family history revealed no other members suffering from any eye diseases. On initial examination, his best-corrected visual acuity was 0.9 in the right eye and 0.6 in the left eye. Humphrey static perimetry revealed a severe decrease in sensitivity within the central 30 degrees of the visual field in both eyes (Fig. 1A). Dark-adaptometry of this patient showed a loss of the rod branch. The cone threshold was within normal range. Ophthalmoscopy showed a nearly normal fundus appearance except for slight hypopigmentation at the macula of the left eye, which may be due to age-related changes in the retinal pigment epithelium (Fig. 1B), but fluorescein angiography demonstrated periphlebitis of the retinal vessels (arrows, Fig. 1C). Spectral-domain optical coherence tomography (SD-OCT) showed that the morphology of the retina was normal in both eyes (Fig. 1D).

Electrophysiological examinations

Recordings of the full-field ERGs from this patient showed that the rod responses were undetectable (Fig. 2). The rod- and cone-mixed maximal response was a negative-type with an a-wave of normal amplitude and a b-wave that was smaller than the a-wave. The a-wave of the cone response had a wide trough, and the b-wave was reduced by 40%. The amplitude of the 30-Hz flicker ERG was reduced by 50%. The photopic long-flash ERG showed severely reduced ON response and normal OFF response. These ERG findings indicated that there was a defect in the signal transmission from photoreceptors to ON bipolar cells both in both rod and cone pathways.

Based on these ophthalmological and electrophysiological tests, we suspected that this patient might have PR and referred him to an internist. The general physical examination including positron emission tomography and computed tomography revealed two abnormal masses in the right lung. Biopsy of these masses confirmed that the masses were small cell carcinomas of the lung.

Detection of autoantibodies against TRPM1 in the serum of the CAR patient

Based on our ERG examination results, we hypothesized that the serum of this CAR patient may contain autoantibodies against

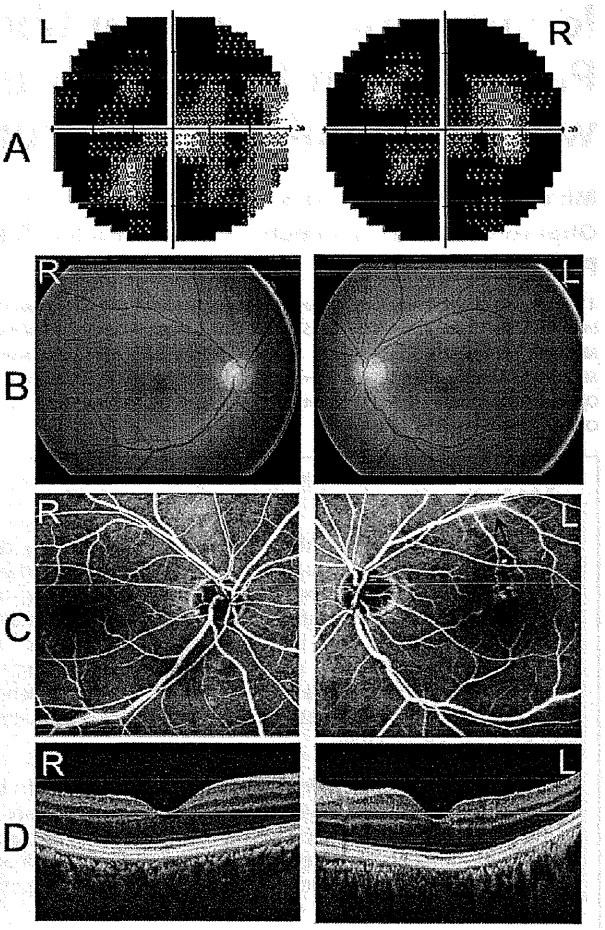

Figure 1. Ophthalmological findings from a patient with paraneoplastic retinopathy (PR) associated with lung cancer. (A) Threshold of static visual field (Humphrey, 30-2 program) plotted on a gray scale showing severely decreased sensitivities within the central 30 degrees of the visual field. (B) Fundus photographs of the patient showing a nearly normal fundus. (C) Fluorescein angiograms showing periphlebitis of the retinal vessels (arrows). (D) Spectral-domain optical coherence tomographic (SD-OCT) image of a 9 mm horizontal scan of the retina of our patient. The retinal structure in each retinal layer is normal.
doi:10.1371/journal.pone.0019911.g001

TRPM1. To test this hypothesis, we examined whether or not this CAR patient's serum could recognize human TRPM1 protein by Western blot analysis. We transfected an expression plasmid containing human TRPM1 cDNA with the C-terminal 3xFlag-tag (TRPM1-3xFlag) into HEK293T cells, and carried out a Western blot analysis using whole cell extracts harvested after 48 hrs cell growth. We first confirmed that TRPM1-3xFlag was expressed by cell using Western blot analysis and an anti-Flag antibody. We detected the ~200 kDa TRPM1-3xFlag band in the cell lysates (Fig. 3A).

Next, we performed Western blot analysis on the same lysates using the serum from our CAR patient and a healthy control person. We detected immunostaining of the same size protein, which was confirmed with the anti-Flag antibody, and with CAR serum. The control serum did not present a significant band (Fig. 3B, C). This result showed the presence of autoantibodies against TRPM1 in this CAR patient's serum.

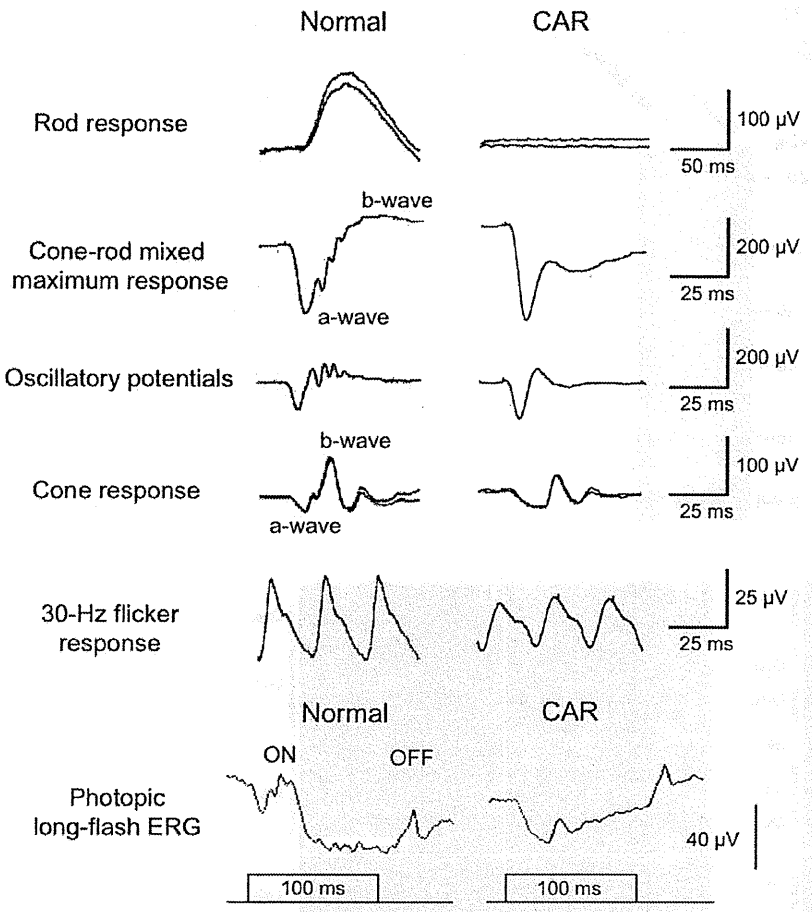

Figure 2. Full-field ERG recordings. The rod response was recorded with a blue light at an intensity of 5.2×10^{-3} cd-s/m^2 after 30 minutes of dark-adaptation. The cone-rod mixed maximum response was elicited by a white flash at an intensity of 44.2 cd-s/m^2. The oscillatory potentials were recorded with a white flash at an intensity of 44.2 cd-s/m^2 using a band-pass filter of 50–1000 Hz. The cone response and a 30 Hz flicker response were elicited by a white stimulus of 4 cd-s/m^2 and 0.9 cd-s/m^2, respectively, on a blue background of 30 cd/m^2. Photopic long-flash ERG responses were also elicited by long-duration flashes of 100 ms using a densely-packed array of white LEDs of 200 cd/m^2 on a white background of 30 cd/m^2.
doi:10.1371/journal.pone.0019911.g002

To examine whether the serum from the CAR patient recognized retinal bipolar cells, we carried out an immunohistochemical analysis on monkey and mouse retinas. We first performed immunohistochemistry on the retina of a 3-year-old rhesus monkey (*Macaca mulata*) and on the retina of a one-month-old C57/B6 mouse using the serum of the CAR patient, however, we did not obtain a significant staining signal above background (data not shown). We then concentrated the serum by IgG purification followed by filter spin column centrifugation and performed immunohistochemistry on the monkey retina using the concentrated serum (Fig. 3D–G). We observed a significant immunolabeling on the INL in the monkey retina (Fig. 3D, F) whereas the normal serum did not give a significant labeling (Fig. 3E, G). The antibodies immuolabeled both the bipolar side and amacrine side of the INL. Since most of the cells residing on the outer side of the INL are ON bipolar cells, at least some of the stained cells are ON bipolar cells. It should be noted some of the staining signals show a spotted pattern in the outer plexiform layer (Fig. 3F) as is observed in TRPM1 or mGluR6 immunostaining on the mouse retina [13], suggesting that the CAR patient serum recognizes the bipolar dendritic tips where some of the TRPM1 protein localizes.

Western blot analysis of the sera from MAR patients

Since the functional defect in the retina of MAR patients is known to be due to abnormal signal transmission between photoreceptors and ON bipolar cells [8,9], we then investigated whether or not autoantibodies to TRPM1 were also present in the sera of MAR patients. We obtained the sera of 26 MAR patients from two hospitals in Japan (Chiba University Hospital and Iwate Medical University Hospital) and Ocular Immunology Laboratory in the USA (Casey Eye Institute). We found that the sera from patients #8 and #23 exhibited a significant immunoreactive band against TRPM1-transfected cell lysates by Western blot analysis (Fig. 4A and B). The control serum showed no significant immune response against the TRPM1-transfected cell lysates (Fig. 3C). These results suggest that the sera from some MAR patients contain autoantibodies against TRPM1. Due to the limited volume of sera from the MAR patients, we could not try immunostaining on the monkey or the mouse retina using the serum from the patients #8 and #23.

MAR patient #8, was a 76-year-old man with a history of skin melanoma. He had ring scotomas and abnormal ERGs indicating that he had MAR. The other patient, MAR #23, was a 57-year-

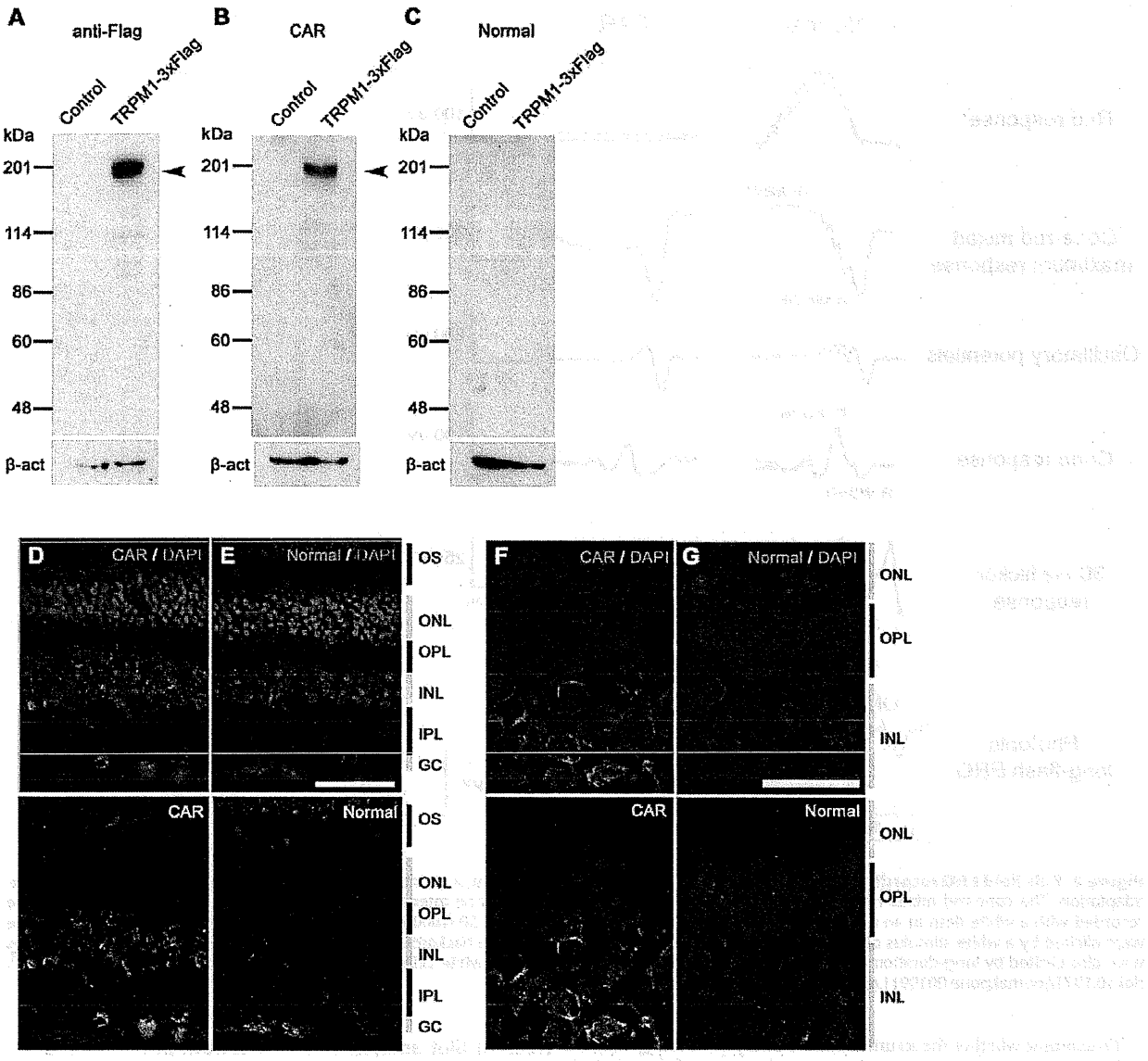

Figure 3. Immunostaining and Western blot analysis of human TRPM1 using serum from the CAR patient. (A–C) Immunoblots of the transfected cell lysates using an antibody against Flag tag (A), serum from CAR patient (B), and control serum (C). Arrowheads indicate the TRPM1-3xFlag protein bands. HEK293T cells were transfected with the pCAGGS or pCAGGS-human TRPM1-3xFlag plasmid, and cells were harvested after 48 hrs. β-actin (β-act) was used for a loading control. (D–G) Confocal images of a three-year-old rhesus monkey retina immunostained with the concentrated serum from the CAR patient (D, F) or the concentrated normal serum (E, G). Cell nuclei are visualized with DAPI. CAR patient serum presented signals on INL cells and the inner part of the OPL (D, F). Scale bar = 50 μm in (E) and 20 μm in (G).
doi:10.1371/journal.pone.0019911.g003

old man with poor night vision, abnormal scotopic ERGs and abnormal color vision. He had a history of skin melanoma and thyroid cancer. There was no other clinical information available on these two patients because these sera were obtained from other institutes several years before without detailed clinical information.

Discussion

PR, including MAR and CAR, presents visual disorders associated with systemic cancer. Antibodies against retinal cells and proteins have been detected in the sera of patients with PR suggesting an autoimmune basis for the etiology of the PR. The autoantibodies identified so far include rhodopsin, retinal transducin alpha and beta, recoverin, S-arrestin, α-enolase, carbonic anhydrase II, and heat shock protein-60 which reside abundantly in photoreceptors [1–10,16]. MAR and CAR can cause bipolar cell dysfunction [7–12]. The results of the ERG [8,9] and immunohistochemistry [7] studies suggested that the main target of MAR are retinal ON bipolar cells in both the rod and cone pathways. However, autoantibodies specifically reacting with a bipolar cell antigen had not been identified in the sera of patients with PR, including those with CAR and MAR. In the current study, we identified autoantibodies against TRPM1, a component of the ON bipolar cell transduction channel negatively regulated by Goα in the mGluR6 signaling pathway [13–15], in the

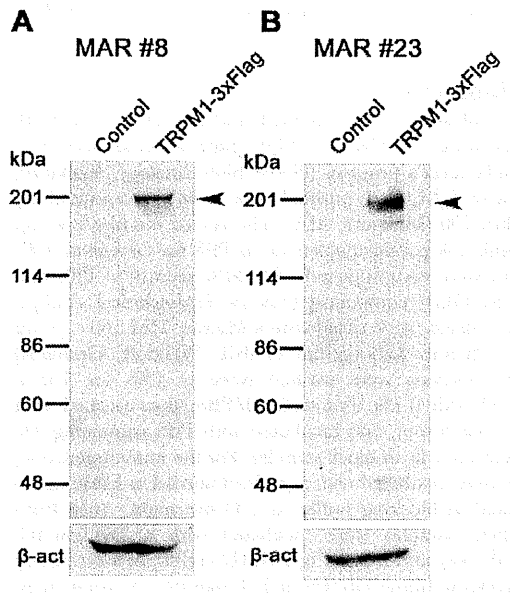

Figure 4. Western blot analysis of human TRPM1 using sera from the MAR patients. (A, B) Immunoblots of the transfected cell lysates using sera from MAR patient #8 (A) and MAR patient #23 (B). HEK293T cells were transfected with pCAGGS or pCAGGS-human TRPM1-3xFlag plasmid, and cells were harvested after 48 hrs. Arrowheads indicate the TRPM1-3xFlag protein bands. β-actin (β-act) was used for a loading control.
doi:10.1371/journal.pone.0019911.g004

sera of one CAR patient and two MAR patients. The CAR patient exhibited a dysfunction of ON bipolar cells, and to our knowledge, this is the first report on an autoantibody against a bipolar cell antigen in the serum of PR patients affecting the ON bipolar cell function.

Previously, we isolated a mouse *TRPM1-L* cDNA corresponding to the human long form of *TRPM1*, and found that the TRPM1-L protein is developmentally localized at the tips of the ON bipolar dendrites co-localizing with mGluR6, but not on OFF bipolar cells [13,14]. The *TRPM1* null mutant mouse completely loses the ON bipolar cell photoresponses to light, indicating that TRPM1 plays a critical role in the synaptic transmission from photoreceptors to ON-bipolar cells [13,15]. In addition, we demonstrated using a CHO cell reconstitution system that TRPM1-L is a nonselective cation channel which is negatively regulated by Goα downstream of the mGluR6 signaling cascade in ON bipolar cells [13]. Recently, four groups including ours independently reported that mutations of human *TRPM1* are associated with the complete-type of congenital stationary night blindness (cCSNB), an inherited human retinal disease [17–20]. cCSNB is a non-progressive retinal disease characterized by congenital night blindness with a moderate decrease in visual acuity and myopia [21-24]. Previous ERG studies have suggested that the defect in cCSNB patients lies in the signal transmission from photoreceptors to ON bipolar cells in both the rod and cone pathways [25–28]. We have identified five different mutations in our three cCSNB patients, and have shown that these mutations lead to either abnormal TRPM1 protein production or mislocalization of the TRPM1 protein in bipolar cell dendrites [17]. These results suggest that TRPM1 plays a critical role in mediating the photoresponses of ON bipolar cells in humans as well. Based on these findings, we hypothesize that the ectopic expression of TRPM1 in tumor cells of some CAR and MAR patients may result in aberrant production of autoantibodies to TRPM1 through B-lymphocytic responses [29–32]. These antibodies may react to the TRPM1 protein in retinal ON bipolar cells resulting in dysfunction of the TRPM1 transduction cation channel downstream of the mGluR6 signaling cascade. However, we could not confirm whether TRPM1 is expressed in the tumor cells of the three PR patients examined in this study [29] because tumor samples were not available.

Another question regarding the disease mechanism underlying PR is whether the binding of TRPM1 autoantibody to bipolar cells results in the cell death or dysfunction of bipolar cells. As far as we examined the retinal structure of the CAR patient using a spectral domain optical coherence tomography (SD-OCT) retinal imaging device, the structure of the retinal bipolar cell layer appeared to be well preserved even three months after the onset of symptoms (Fig. 1D). This suggests that the autoantibodies reacting to TRPM1 cause dysfunction of the ON bipolar transduction pathway rather than bipolar cell death. However, further studies are needed to clarify the exact disease mechanism.

In the sera of MAR patients, several types of autoantibodies against retinal proteins have been reported, including the 22 kDa neuronal antigen GNB1, rhodopsin, S-arrestin, and aldolase-A and -C [10,16,33,34]. We initially considered that TRPM1 might be a major MAR target antigen, because TRPM1 is exclusively expressed in retinal ON bipolar cells. However, autoantibodies against TRPM1 were detected in only two out of 26 MAR. patients' sera (7.7%, Fig. 4A, B). We tested whether the sera of one CAR patient and 26 MAR patients recognized human mGluR6, which is specifically expressed in ON bipolar cells, however, none of the sera exhibited a significant band in Western blot analysis (data not shown). Thus, antigens other than TRPM1 or mGluR6 may be involved in the pathogenesis of a large proportion of MAR.

Immunohistochemical analyses using the serum of the CAR patient showed labeling in the inner nuclear layer and outer plexiform layer of the adult rhesus monkey retina (Fig. 3D–G), where the bipolar cell bodies and dendrites reside, respectively. This immunostaining pattern is somewhat similar to our previous immunostaining results on the mouse retina with specific antibody against mouse TRPM1-L, which corresponds to the human TRPM1 long form [13]. Other labeling was also observed in the amacrine cells and ganglion cells. The reason for the immunoreactivity with these cells is uncertain, however, it may be due to the presence of other autoantibodies against amacrine cell and ganglion cell antigens. Lu *et al.* reported the presence of various different autoantibodies in the serum of a single PR patient [10]. If this is the case, it may explain why our CAR patient displayed severely reduced visual sensitivities in the visual field tests (Fig. 1A) unlike cCSNB patients with TRPM1 mutations [17].

It should be noted that we did not confirm whether there are any antoantibodies against TRPM1 in the sera of normal subjects by using a large number of samples. However, this possibility is thought to be low, because Shimazaki *et al.* reported that the molecular weights of the IgGs with observed anti-retinal reactivity in 92 normal sera were smaller than 148 kDa, which is smaller than the TRPM1 molecular weight of ~200 kDa, although relatively high molecular weight reactivity was not intensively investigated [35].

One limitation of the current study is that we could not obtain detailed information on the two MAR patients, MAR #8 and #23, associated with the TRPM1 autoantibody. We confirmed that these two patients had skin melanomas accompanying the visual disturbances, but could not obtain a more detailed clinical history or data on visual acuity, visual field, or ERGs because these sera were sent from different hospitals several years ago. Thus, we do not know whether these two MAR patients really had retinal ON bipolar cell dysfunction. Further prospective studies of the TRPM1 autoantibodies in large numbers of MAR patients are needed.

In conclusion, our study suggests that TRPM1 may be one of the causative antigens responsible for PR associated with ON bipolar cell dysfunction.

Note added in proof

During the course of revision process of this manuscript, Dhingra *et al.* (J. Neurosci. 31, 3962–3967, 2011) independently reported the presence of autoantibodies against TRPM1 in two MAR patients. Our study reports on autoantibodies against TRPM1 in CAR serum in addition to MAR sera.

Materials and Methods

Subjects

The Nagoya University Hospital Ethics Review Board approved this study (approval ID 1131). Of the PR patients that were examined in the Nagoya University Hospital, one PR patient with lung cancer and ON bipolar cell dysfunction was studied in detail. The examinations included routine ophthalmological and electrophysiological tests. In addition, immunohistochemical and Western blot analyses were performed using the serum of this patient. The procedures used conformed to the tenets of the Declaration of Helsinki of the World Medical Association. A written informed consent was obtained from the patient after he was provided with sufficient information on the procedures to be used.

We also obtained sera of 26 patients with MAR from two hospitals in Japan (Chiba University Hospital and Iwate Medical University Hospital) and Ocular Immunology Laboratory in the USA (Casey Eye Institute) for Western blot analysis.

Ophthalmologic examinations

The ophthalmologic examination included best-corrected visual acuity, biomicroscopy, ophthalmoscopy, fundus photography, fluorescein angiography, static perimetry, and spectral-domain optical coherence tomography (SD-OCT). Static visual fields were obtained with the Humphrey 30-2 program (Carl Zeiss, Dublin, USA), and the results are shown in gray scale. SD-OCT was performed with a 9-mm horizontal scan through the midline with 50 averages (Spectralis HRA+OCT; Heidelberg Engineering, Vista, CA).

Electroretinograms (ERG)

Full-field ERGs were elicited with a Ganzfeld dome and recorded with a Burian-Allen bipolar contact lens electrode. The ground electrode was attached to the ipsilateral ear.

After 30 minutes of dark-adaptation, a rod response was elicited with a blue light at an intensity of 5.2×10^{-3} cd-s/m^2. A cone-rod mixed maximum response was elicited by a white flash at an intensity of 44.2 cd-s/m^2. A cone response and a 30 Hz flicker response were elicited by a white stimulus of 4 cd-s/m^2 and 0.9 cd-s/m^2, respectively, on a blue background of 30 cd/m^2. Full-field cone ERGs were also elicited by long-duration flashes of 100 ms using a densely packed array of white LEDs. The array was positioned at the top of the Ganzfeld dome and covered by a diffuser. The stimulus intensity and background illumination measured in the dome was 200 cd/m^2 and 30 cd/m^2, respectively. Responses were amplified by 10K and the band pass was set to 0.3 to 1000 Hz. The data were digitized at 4.3 kHz, and 5 to 20 responses were averaged (Neuropack, Nihonkohden, Tokyo, Japan).

Immunohistochemistry

For immunohistochemistry, patient and normal sera (300 µl) were purified using the Melon Gel IgG purification kit according to the manufacturer's protocol (Pierce Biotechnology, Rockford, IL) to remove IgM, and purified sera were concentrated by Amicon Ultra 100 (Millipore, MA). The rhesus monkey eye cup was fixed with 4% paraformaldehyde in PBS for 30 min at 4°C. The samples were cryoprotected with 30% sucrose in PBS and embedded in OCT compound (Sakura Finetechnical, Tokyo, Japan). These tissues were sliced with a Microm HM 560 cryostat microtome (Microm Laborgeräte GmbH, Walldorf, Germany) into 14 µm. Sections were washed twice in PBS for 5 min, permeabilized with 0.1% Triton-X100/PBS, then washed with PBS 3 times for 5 min, and incubated with PBS containing 4% donkey serum for 1 hr to block samples. For the immunoreaction, the samples were incubated with a purified normal or CAR serum (1:300) diluted in blocking buffer at 4°C overnight. After PBS-washing, these samples were incubated with a DyLight-488 conjugated donkey anti-human IgG (H+L) (1:400) as a secondary antibody (Jackson Immunoresearch Laboratories) at room temperature for 1 hr and washed with PBS.

Transfection and Western blot analyses

HEK293T cells were cultured in D-MEM containing 10% fetal bovine serum (FBS; Nissui, Tokyo, Japan). These cells were grown under 5% carbon dioxide at 37°C. The calcium phosphate method was used to transfect the cells. Transfected cells were incubated at 37°C for 48 hrs, and then harvested for further analysis. The proteins extracted from the cells were separated by SDS–PAGE on a 7.5% precast gel (ATTO, Tokyo, Japan), and then transferred to a polyvinylidene difluoride membrane using the Invitrogen iBlot system (Invitrogen, Carlsbad, CA, USA). The membrane was incubated with primary antibodies, mouse anti-Flag (1:1,000; Sigma, St Louis, MO), sera from patients (1:100), normal human serum (1:100), or mouse anti-β-actin (1:5,000; Sigma). The membrane was then incubated with a horseradish peroxidase-conjugated goat anti-mouse IgG (1:10,000; Zymed Laboratories, San Francisco, CA) or donkey anti-human IgG (1:10,000; Jackson Immuno Research Laboratories, West Grove, PA) as secondary antibodies. The bands were developed using Chemi-Lumi One L (Nacalai Tesque, Kyoto, Japan).

Acknowledgments

We thank Richaed G. Weleber, Yozo Miyake, and Duco I. Hamasaki for helpful discussions of this study, Junko Hanaya for collecting the serum of our patients, and Mikiko Kadowaki, Aiko Ishimaru, Kaori Sone, and Shawna Kennedy for technical assistance.

Author Contributions

Conceived and designed the experiments: MK TF. Performed the experiments: MK RS SU YN NH. Analyzed the data: MK RS SU TF. Contributed reagents/materials/analysis tools: MK SU HO SY SM HT GA. Wrote the paper: MK TF. Supervised the project: MK HT TF.

References

1. Thirkill CE, FitzGerald P, Sergott RC, Roth AM, Tyler NK, et al. (1989) Cancer-associated retinopathy (CAR syndrome) with antibodies reacting with retinal, optic-nerve, and cancer cells. N Engl J Med 321: 1589–1594.
2. Chan JW (2003) Paraneoplastic retinopathies and optic neuropathies. Surv Ophthalmol 48: 12–38.
3. Heckenlively JR, Ferreyra HA (2008) Autoimmune retinopathy: A review and summary. Semin Immunopathol 30: 127–134.
4. Adamus G (2009) Autoantibody targets and their cancer relationship in the pathogenicity of paraneoplastic retinopathy. Autoimmun Rev 8: 410–414.

5. Thirkill CE, Roth AM, Keltner JL (1987) Cancer-associated retinopathy. Arch Ophthalmol 105: 372–375.
6. Jacobson DM, Thirkill CE, Tipping SJ (1990) A clinical triad to diagnose paraneoplastic retinopathy. Ann Neurol 28: 162–167.
7. Milam AH, Saari JC, Jacobson SG, Lubinski WP, Feun LG, et al. (1993) Autoantibodies against retinal bipolar cells in cutaneous melanoma-associated retinopathy. Invest Ophthalmol Vis Sci 34: 91–100.
8. Alexander KR, Fishman GA, Peachey NS, Marchese AL, Tso MOM (1992) "On" response defect in paraneoplastic night blindness with cutaneous malignant melanoma. Invest Ophthalmol Vis Sci 33: 477–483.
9. Lei B, Bush RA, Milam AH, Sieving PA (2000) Human melanoma-associated retinopathy (MAR) antibodies alter the retinal ON-response of the monkey ERG in vivo. Invest Ophthalmol Vis Sci 41: 262–266.
10. Lu Y, Jia L, He S, Hurley MC, Leys MJ, et al. (2009) Melanoma-associated retinopathy: a paraneoplastic autoimmune complication. Arch Ophthalmol 127: 1572–1580.
11. Jacobson DM, Adamus G (2001) Retinal anti-bipolar cell antibodies in a patient with paraneoplastic retinopathy and colon carcinoma. Am J Ophthalmol 131: 806–808.
12. Goetgebuer G, Kestelyn-Stevens AM, De Laey JJ, Kestelyn P, Leroy BP (2008) Cancer-associated retinopathy (CAR) with electronegative ERG: a case report. Doc Ophthalmol 116: 49–55.
13. Koike C, Obara T, Uriu Y, Numata T, Sanuki R, et al. (2010) TRPM1 is a component of the retinal ON bipolar cell transduction channel in the mGluR6 cascade. Proc Natl Acad Sci U S A 107: 332–337. Epub Dec. 4, 2009.
14. Koike C, Numata T, Ueda H, Mori Y, Furukawa T (2010) TRPM1: A vertebrate TRP channel responsible for retinal ON bipolar function. Cell Calcium 48: 95–101.
15. Morgans CW, Zhang J, Jeffrey BG, Nelson SM, Burke NS, et al. (2009) TRPM1 is required for the depolarizing light response in retinal ON-bipolar cells. Proc Natl Acad Sci U S A 106: 19174–19178.
16. Hartmann TB, Bazhin AV, Schadendorf D, Eichmüller SB (2005) SEREX identification of new tumor antigens linked to melanoma-associated retinopathy. Int J Cancer 114: 88–93.
17. Nakamura M, Sanuki R, Yasuma TR, Onishi A, Nishiguchi KM, et al. (2010) TRPM1 mutations are associated with the complete form of congenital stationary night blindness. Mol Vis 16: 425–437.
18. Li Z, Sergouniotis PI, Michaelides M, Mackay DS, Wright GA, et al. (2009) Recessive mutations of the gene TRPM1 abrogate ON bipolar cell function and cause complete congenital stationary night blindness in humans. Am J Hum Genet 85: 711–719.
19. van Genderen MM, Bijveld MM, Claassen YB, Florijn RJ, Pearring JN, et al. (2009) Mutations in TRPM1 are a common cause of complete congenital stationary night blindness. Am J Hum Genet 85: 730–736.
20. Audo I, Kohl S, Leroy BP, Munier FL, Guillonneau X, et al. (2009) TRPM1 is mutated in patients with autosomal-recessive complete congenital stationary night blindness. Am J Hum Genet 85: 720–729.
21. Miyake Y, Yagasaki K, Horiguchi M, Kawase Y, Kanda T (1986) Congenital stationary night blindness with negative electroretinogram: A new classification. Arch Ophthalmol 104: 1013–1020.
22. Bech-Hansen NT, Naylor MJ, Maybaum TA, Sparkes RL, Koop B, et al. (2000) Mutations in NYX, encoding the leucine-rich proteoglycan nyctalopin, cause X-linked complete congenital stationary night blindness. Nat Genet 26: 319–23.
23. Pusch CM, Zeitz C, Brandau O, Pesch K, Achatz H, et al. (2000) The complete form of X-linked congenital stationary night blindness is caused by mutations in a gene encoding a leucine-rich repeat protein. Nat Genet 26: 324–327.
24. Dryja TP, McGee TL, Berson EL, Fishman GA, Sandberg MA, et al. (2005) Night blindness and abnormal cone electroretinogram ON responses in patients with mutations in the GRM6 gene encoding mGluR6. Proc Natl Acad Sci USA 102: 4884–4889.
25. Miyake Y, Yagasaki K, Horiguchi M, Kawase Y (1987) On- and off-responses in photopic electroretinogram in complete and incomplete types of congenital stationary night blindness. Jpn J Ophthalmol 31: 81–87.
26. Houchin K, Purple RL, Wirtschafter JD (1991) X-linked congenital stationary night blindness and depolarizing bipolar system dysfunction. [ARVO abstract]. Invest Ophthalml Vis Sci 32: S1229.
27. Young RSL (1991) Low-frequency component of the photopic ERG in patients with X-linked congenital stationary night blindness. Clin Vis Sci 6: 309–315.
28. Khan NW, Kondo M, Hiriyanna KT, Jamison JA, Bush RA, et al. (2005) Primate retinal signaling pathways: Suppressing ON-pathway activity in monkey with glutamate analogues mimics human CSNB1-NYX genetic night blindness. J Neurophysiol 93: 481–492.
29. Polans AS, Witkowska D, Haley TL, Amundson D, Baizer L, et al. (1995) Recoverin, a photoreceptor-specific calcium-binding protein, is expressed by the tumor of a patient with cancer-associated retinopathy. Proc Natl Acad Sci U S A 92: 9176–9180.
30. Matsubara S, Yamaji Y, Sato M, Fujita J, Takahara J (1996) Expression of a photoreceptor protein, recoverin, as a cancer-associated retinopathy autoantigen in human lung cancer cell lines. Br J Cancer 74: 1419–1422.
31. Ohguro H, Odagiri H, Miyagawa Y, Ohguro I, Sasaki M, et al. (2004) Clinicopathological features of gastric cancer cases and aberrantly expressed recoverin. Tohoku J Exp Med 202: 213–219.
32. Bazhin AV, Schadendorf D, Willner N, De Smet C, Heinzelmann A, et al. (2007) Photoreceptor proteins as cancer-retina antigens. Int J Cancer 120: 1268–76.
33. Keltner JL, Thirkill CE (1999) The 22-kDa antigen in optic nerve and retinal diseases. J Neuroophthalmol 19: 71–83.
34. Potter MJ, Adamus G, Szabo SM, Lee R, Mohaseb K, et al. (2002) Autoantibodies to transducin in a patient with melanoma-associated retinopathy. Am J Ophthalmol 134: 128–30.
35. Shimazaki K, Jirawuthiworavong GV, Heckenlively JR, Gordon LK (2008) Frequency of anti-retinal antibodies in normal human serum. J Neuro-Ophthalmol 28: 5–11.

Stiles–Crawford effect in focal macular ERGs from macaque monkey

Celso Soiti Matsumoto — Department of Ophthalmology, Faculty of Medicine, Oita University, Oita, Japan, Department of Ophthalmology, Teikyo University School of Medicine, Tokyo, Japan, & Matsumoto Eye Clinic, Tokushima, Japan

Kei Shinoda — Department of Ophthalmology, Teikyo University School of Medicine, Tokyo, Japan

Harue Matsumoto — Matsumoto Eye Clinic, Tokushima, Japan

Shingo Satofuka — Department of Ophthalmology, Teikyo University School of Medicine, Tokyo, Japan

Atsushi Mizota — Department of Ophthalmology, Teikyo University School of Medicine, Tokyo, Japan

Kazuo Nakatsuka — Shonin Hospital, Oita, Japan

Yozo Miyake — Aichi Medical University, Aichi, Japan

Background: To determine whether the focal macular electroretinograms (FMERGs) are affected by the angle of incidence of the stimulating light on the retina, i.e., the Stiles–Crawford effect (SCE). *Methods*: FMERGs were elicited by focal stimulation of the macula in three light-adapted macaque monkeys. The incidence of the light on the retina was varied from 0 to ±11.7°. The effects of the incidence and wavelengths of the stimulus on the SCE were determined. *Results*: The amplitudes of the FMERG components were largest when the stimulus beam entered the eye on the visual axis and passed through the center of the pupil. The amplitudes gradually decreased as the stimulus beam passed through the pupil more eccentrically and fell on the retina more obliquely. All components of the FMERGs were decreased with the decrease least for the amplitude of the d-wave. *Conclusions*: The decrease in the amplitudes of the FMERGs as the angle of incidence of the stimulus beam on the retina increases demonstrates that the SCE can be detected in adult macaque monkeys. This objective method of assessing the SCE suggests that this technique can be used to assess the alignment of cones in humans with different types of macular diseases.

Keywords: Stiles–Crawford effect, focal macular electroretinogram, ERG

Citation: Matsumoto, C. S., Shinoda, K., Matsumoto, H., Satofuka, S., Mizota, A., Nakatsuka, K., & Miyake, Y. (2012). Stiles–Crawford effect in focal macular ERGs from macaque monkey. *Journal of Vision, 12*(3):6, 1–7, http://www.journalofvision.org/content/12/3/6, doi:10.1167/12.3.6.

Introduction

Focal macular electroretinograms (FMERGs) have been used to assess the physiological condition of different retinal neuronal cells including the photoreceptors in the macular area (DeLint, Berendschot, & van Norren, 1998; Kondo, Miyake, Horiguchi, Suzuki, and Tanikawa, 1998). In most experimental and clinical studies, FMERGs have been recorded, and the effects of the Stiles–Crawford effect (SCE), a decrease in the luminous efficiency of light entering the edge of the pupil, were not examined. However with focal stimulation, the direction of the incidence beam becomes more important.

Evidence has been obtained that the directional sensitivity of the cones to light stimuli is responsible for the SCE (Alpern, 1986; Alpern, Kitahara, & Fielder 1987; Alpern & Kitahara, 1983; Stiles & Crawford, 1933). The SCE is generally determined by psychophysical tests (Alpern, 1986; Alpern et al., 1987; Alpern & Kitahara, 1983; DeLint, Vos, Berendoschot, & van Norren, 1997), and the subjects are required to actively participate in the examination. Thus, high level of concentration and good visual acuity are required to perform the tests.

doi: 10.1167/12.3.6 **Received** June 11, 2011; published March 6, 2012 ISSN 1534-7362 © ARVO

The SCE has been examined objectively in humans by only a few investigators. DeLint et al. analyzed the SCE by measuring the visual pigment density with different incidences of the bleaching and reflected light (DeLint et al., 1998). Birch et al. stimulated focal macular areas with a steady-state flickering light through a two-channel Maxwellian-view optical system to elicit focal ERGs (Birch, Sandberg, & Berson, 1982). They showed that the SCE could be demonstrated at the fovea in normal subjects. However, they isolated the b-waves by using band-pass filters, and a separation of a-wave and d-wave components was not possible. The FMERGs in our study enabled us to isolate the a-, b-, and d-waves, and we were able to analyze each component to determine whether each showed the SCE effect.

We have developed an FMERG system that is integrated into a slit lamp that allowed us to stimulate the retina with a spot of light at any incidence (Choshi, Matsumoto, & Nakatsuka, 2003; Yamada, Matsumoto, & Nakatsuka, 2006). This FMERG stimulating and recording system prompted us to assess the SCE objectively with long-duration stimuli. This system allowed the ERG recordings to be performed under direct fundus observation, and each component of the FMERGs could be analyzed separately.

Thus, the purpose of this study was to determine whether the SCE was present in the foveal area of macaque monkeys. To accomplish this, we elicited FMERGs from three macaque monkeys by light of different incidences on the retina. We shall show that all components of the FMERGs were affected by the SCE with the d-wave least affected.

Materials and methods

Animals

Focal macular ERGs (FMERGs) were recorded from 3 eyes of 3 adult (ages 6, 6, and 8 years) male macaque monkeys (*Macaca fuscata*). All experimental and animal care procedures adhered to the ARVO Statement for the Use of Animals in Ophthalmic and Vision Research and were approved by the Institutional Animal Care Committee of Oita University.

FMERG recordings

The monkeys were initially anesthetized by an intramuscular injection of a mixture of ketamine (7 mg/kg), xylazine (0.6 mg/kg), and butorphanol tartrate (0.04 mg/kg) and maintained on an infusion of the same proportions of ketamine, xylazine, and butorphanol tartrate per hour. The depth of the anesthesia was maintained at a level sufficient to inhibit the corneal reflex and eye movements. The pupils were dilated with topical tropicamide (0.5%) and phenylephrine hydrochloride (5%), and the cornea was anesthetized with topical oxybuprocaine hydrochloride (0.4%). The non-stimulated eye was covered with an opaque patch.

Photopic stimuli

An optical system was built to deliver focal stimuli to the macula under direct fundus observation. The system was designed so that the stimulus light passed through the center of the pupil, i.e., on the visual axis, or through different parts of the pupil from the temporal to nasal edge in 0.5-mm steps. The light sources were from hyper-bright light-emitting diodes (LEDs; NSPW500BS, NICHIA, Tokushima, Japan), and the stimuli positioning unit was a motorized helicoid stage (Sigma Koki, Saitama, Japan) with a telescopic optical system mounted on the stage. The stage moved the telescope so that the stimulating beam entered the pupil from the temporal to nasal sides across the visual axis in 0.5-mm steps. The movement of the stage had an accuracy of 0.05 mm.

The fundus observation system was composed of a near-infrared CCD camera (Hitachi, Japan) integrated on a customized slit lamp microscope (Carl-Zeiss, Germany). The position of the light spot on the macular area was monitored during all of the recordings. The stimulus spot was 5° in diameter. To examine the effects of the wavelength of the stimulus on the SCE, red (λ_{max} = 644 nm, half-amplitude bandwidth of 634 to 655 nm, TLRH180P, TOSHIBA, Tokyo, Japan), amber (λ_{max} = 590 nm, half-amplitude bandwidth of 585 to 596 nm, TLYE260A, TOSHIBA, Tokyo, Japan), green (λ_{max} = 523 nm, half-amplitude bandwidth of 512 to 545 nm, SLA580EC4T, ROHM, Kyoto, Japan), and blue (λ_{max} = 470 nm, half-amplitude bandwidth of 460 to 482 nm, NSPB500S, NICHIA, Tokushima, Japan) LEDs were used to elicit the FMERGs.

The white light stimulus intensity was set to 38 cd/m^2. The spectral characteristics (bandwidth and λ_{max}) of the LEDs used in this study were measured with a spectral colorimeter PR-650 SpectraScan and analyzed with SpectraView software (Photoresearch, CA, USA).

To determine whether the ERGs were focal, the 5° stimulus spot was projected onto the optic nerve head, and FMERGs were elicited by decreasing stimulus intensities. The FMERGs recorded by the stimulus projected on the optic nerve head became non-recordable when the intensity was ≤38 cd/m^2 indicating that this stimulus intensity would provide a focal response from the macula with negligible effect of stray light (Choshi et al., 2003; Yamada et al., 2006). The intensity of each colored light stimulus was matched by neutral density filters to elicit approximately the criteria amplitude of b-wave (1 μV) as elicited by the white stimulus whose luminance was

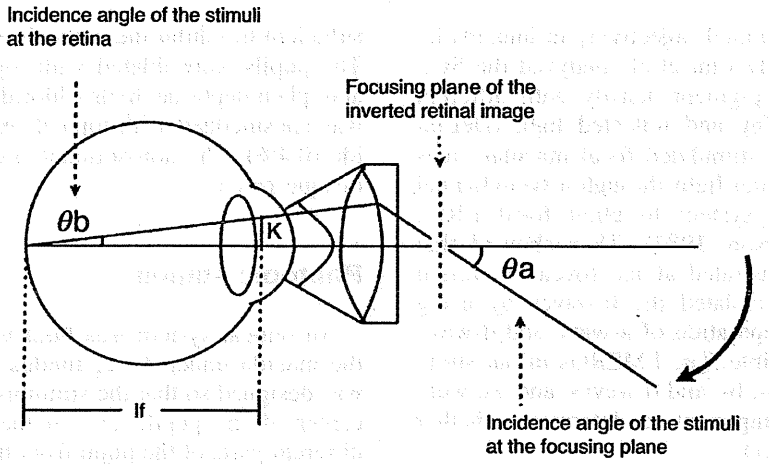

Figure 1. Relationship between the angle of incidence of the light beam on the focusing plane of the inverted retinal image. IF = IF distance, i.e., the axial length minus the corneal thickness and anterior chamber depth and K = distance of the stimulus beam from the visual axis in the iris plane in millimeters.

$\leq$38 cd/m^2. The FMERG waveforms were comprised of on and off waves. The adjusted intensity elicited no ERGs when the stimulus spot was projected onto the optic nerve head.

A gold-foil bipolar contact lens (Mayo, Nagoya, Japan) coupled with a mini-pan fundus lens was placed on the cornea of the examined eye (Figure 1). This provided an inverted real image of the ocular fundus projected approximately 3.5 mm in front of the contact lens unit. The relationship between the angle of incidence of the light beam on the focusing plane of the inverted retinal image and that on the retinal surface was calculated as shown in Figure 1. When the light beam fell on the temporal side of the real image at an angle of θ_a, then the light beam will be projected from the nasal side onto the retinal surface at an angle of θ_b. The relationship between θ_a and θ_b was calculated by

$$[\tan\theta_b = C(\tan\theta_a)], \quad (1)$$

with θ_b being the angle of incidence on the retina, θ_a being the angle of incidence on the focusing plane of the inverted retinal image, and C being the lens magnification constant. Thus, θ_b was determined by the telescope angle and C by the lens magnification constant (0.39).

The distance between the center of the pupil and the stimulus beam was measured as shown in Figure 1. The iris–fovea distance, IF, was calculated by

$$\mathrm{IF} = K/(\tan\theta_b), \quad (2)$$

with K equal to the distance of the light beam from the visual axis in the iris plane, and IF equal to the distance of the axial length with the subtraction of corneal thickness and the anterior chamber depth. A correction for light transmission through the cornea and the lens was not done. The axial length, corneal thickness, and the anterior chamber depth were measured by A-mode ultrasound echography (Compuscan LT, Stortz, St. Louis, MO, USA).

The stimulus duration was 100 ms and the stimulus interval was 150 ms, and thus, the frequency of stimulation was 4 Hz. This stimulus pattern of 100 ms on and 150 ms off was used for each wavelength stimulus. A white light of 35 cd/m^2 for 15 min was used for light adaptation before recording with each wavelength. We believe that the off duration was long enough because the depolarization of the cone is much faster than 150 ms.

FMERG recordings and analyses

A bipolar contact lens electrode (Mayo, Nagoya, Japan) was used to pick up the FMERGs. The ground electrode was attached to the right ear lobe. After centering and focusing the stimulus spot on the macula, the eye was light adapted with 35 cd/m^2 for 15 min. Then, the FMERGs were elicited by different stimulus intensities and wavelengths. The responses were amplified with a NeuropackΣ bioamplifier (MEB-5500, Nihon Kohden, Tokyo), A/D converted at 16 bits (PCI-16/16UD, Contec, Japan), and averaged by a customized signal processing program (MTS, Japan). More than forty responses were averaged, and the sampling rate was 10 kHz (every 0.1 ms). The responses were filtered from 0.5 to 200 Hz with a hardwired band-pass filter. With this system, the noise level with the electrode placed on the cornea and no stimulus was less than 0.1 μV.

The amplitude of the a-wave was measured from the baseline to the trough of the a-wave, and the amplitude of the b-wave was measured from the trough of the a-wave

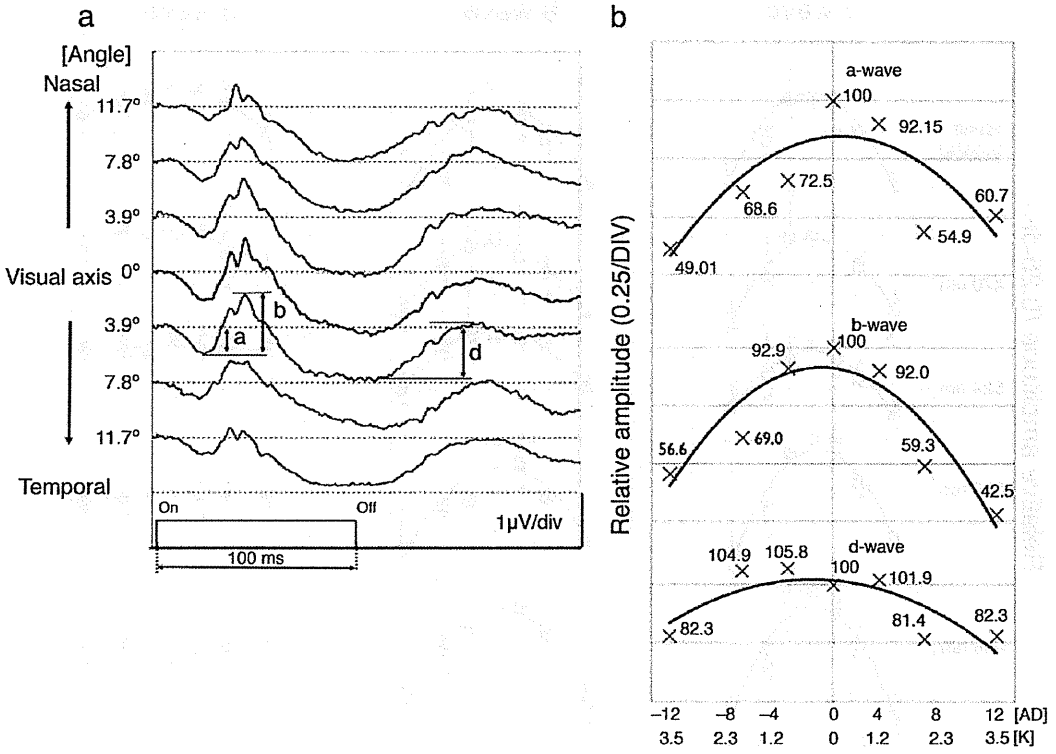

Figure 2. (a) Representative FMERGs elicited by white stimuli entering the pupil at different distances (ordinate) from the visual axis (0) for up to 11.7 degrees. The amplitudes of the a- and b-waves of the FMERGs decrease with increasing distance from the visual axis. (b) The amplitudes of the a-, b-, and d-waves were measured from ERGs such as those from the three monkeys, and the relative amplitudes are plotted on the right. One division of the graph is equal to 25%. *K* represents the distance of the entrance beam to the visual axis in the iris plane in millimeters; AD represents the mean angle of incidence in degrees of stimulus spot from the axis. The blue LED has a peak at 470 nm with a half-amplitude bandwidth between 442 and 520 nm. The green LED has a peak at 523 nm with a half-amplitude bandwidth between 480 and 620 nm. The yellow–orange LED has a peak at 590 nm with a half-amplitude bandwidth between 470 and 620 nm. The red LED has a peak at 644 nm with a half-amplitude bandwidth between 580 and 675 nm.

to the following positive peak (Figure 2). The amplitude of the d-wave was measured from the trough just preceding the d-wave to the positive peak after the stimulus offset.

All of the results are expressed as means ± standard deviations (*SD*s). The polynomial fit of the data was made with the Excel program, ver. 12.0. The polynomial fit was at order 2 for all data.

Results

The amplitudes of the a- and b-waves of the FMERGs were largest when the stimulus beam entered the eye on the visual axis ($K = 0$ mm, retinal angular incidence = 0 degree), and they decreased progressively as the stimulus beam entered more eccentrically up to the edge of the pupil. For example with white light, the average ($n = 3$) relative amplitude of the a-wave at 11.7° was approximately one-half of that at 0°. In the same way, the average ($n = 3$) of the relative amplitude of the b-wave at 11.7° was approximately one-half of that at 0°. Similar changes were found for the d-wave although the degree of change (reduced by 17.7 to 18.6%) was smaller (Figure 2 and Supplementary Table 1). With other wavelengths, the changes depended on the stimulus angle, but the relative amplitude of the d-wave was not evident.

The relative amplitudes of the FMERGs elicited by different wavelengths with peak transmission at 470 nm, 524 nm, 590 nm, and 644 nm are shown in Figure 3. As with the white stimuli, the amplitudes of the a- and b-waves were largest when the light beam entered the pupil on the visual axis and decreased with greater eccentricities. However, the degree of the SCE was not significantly affected by the wavelength of the stimuli (Figure 3).

When the relative amplitude difference was compared between the b-wave and d-wave, significant differences were found for each wavelength used. The relative amplitude differences was calculated as the relative amplitude by the stimulus at 0*K*—that by the stimulus at

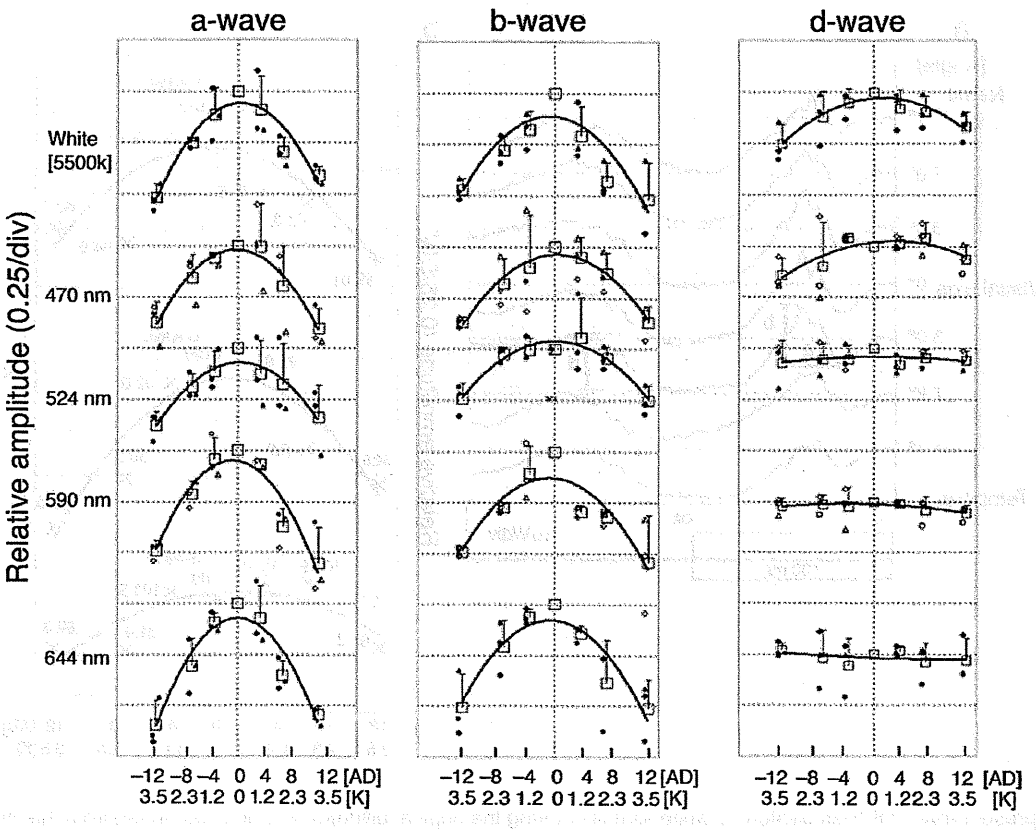

Figure 3. Relative amplitudes of the a-, b-, and d-waves elicited by different wavelengths of the stimulus. The λ_{max} of the stimuli was at 470 nm, 524 nm, 590 nm, and 644 nm. The small symbols (circles, triangles, and asterisks) represent the individual monkeys, the large squares are the averages, and the bars are the standard error of the means. One division of the graph is equal to 25%. *K represents the mean distance of the entrance beam to the visual axis in the iris plane in millimeters; †AD represents the mean angle of incidence in degrees of stimulus spot from the axis.

3.5K (Supplementary Table 1). The relative amplitude difference between maximal incidence stimuli and minimal incidence stimuli was significantly larger for the b-wave than for the d-wave for all wavelengths (Supplementary Table 1). Thus, the d-wave amplitude at the maximal stimulus incidence did not decrease as much as that of the b-wave suggesting that the SCE was larger for the b-waves than for the d-waves.

Discussion

Our results showed that the amplitudes of the a-wave and b-waves of the FMERGs were largest when the stimulus beam entered the eye through the center of the pupil and struck the retina perpendicularly. The amplitudes decreased progressively with increasing eccentricities of the stimulus beam. This is comparable to the SCE obtained psychophysically, and our results demonstrated that the SCE can be measured objectively using the FMERGs to assess the response of the retina.

The SCE is based on the ability of the photoreceptors to absorb photons passing through the outer segments, and the chances of a photon striking a photopigment increase when the beam passes perpendicularly through the entire extent of the outer segments. This explains why the FMERGs are largest when the stimulating beam entered the eye along the visual axis.

More than 25 years earlier, Birch et al. (1982) showed that the SCE can be demonstrated in the focal ERGs elicited by flickering stimuli obtained from a two-channel Maxwellian-view optical system. Our results confirmed their findings and also provided new information on the characteristics of the different components of the ERG and the influence of the wavelength of stimulating light.

Our data showed a drop-off in amplitude of the FMERGs when elicited by stimuli entering the edge of the pupil was approximately 50% whereas it was reported that the decrease of sensitivity was 1 log unit psychophysically (Alpern & Kitahara, 1983) or by OCT (Gao, Cense, Zhang, Jonnal, & Donald, 2008). The discrepancy between perimetry or OCT and the FMERGs is most likely due to methodological differences, i.e., the

FMERGs were elicited by suprathreshold stimulus intensities from focal areas, whereas perimetry employs near threshold stimuli. The FMERGs sum the activity of all of activated cells in the retina, whereas the psychophysical threshold is determined by the activity of the most sensitive cells. An alternative explanation might be that the differences were due to the differences in the species studied.

The degree of the SCE was similar for the a- and b-waves but lower for the d-wave. The origin of each wave is thought to be different. The a- and b-waves receive input from postreceptoral cells including off bipolar cells (Bush & Sieving, 1994) and from on bipolar cell (Sieving, Murayama, & Naarendorp, 1994), respectively. The d-wave arises from the activity of both the photoreceptors and inner retinal neurons (Sieving et al., 1994).

The difference may be due to the distribution of the different types of cones in the macular area (Yamamoto, Gouras, & Lopez, 1995). Another and more likely explanation is that the difference arises from the complexity of the ERG responses with several ERG components interacting. The d-waves of the full-field ERGs result from an interaction of the cone photoreceptor recovery and on bipolar offset and off bipolar cell depolarization. For focal stimuli, the response might be complicated by the photopic negative response (PhNR), because the d-wave is abolished by TTX treatment (Kurimoto et al., 2009; Yamada et al., 2006). Further investigations must be done to determine the reason for the different properties of the d-waves.

Stiles (1937) showed that the SCE depended on the wavelength of the light stimuli, and Alpern and Kitahara (1983) demonstrated that the directional sensitivity parameter (P) is dependent on the wavelength, namely, P was high at short (400 nm) and long (700 nm) wavelengths and lower at middle (550 nm) wavelengths. Our methods were not sensitive enough to detect these differences for the different wavelengths of the stimuli, probably because the bandwidths of the stimuli were relatively broad in our study. This was a limitation of the FMERGs. We used 4 LEDs with different wavelength and white light, while Alpern and Kitahara used 30 different monochromatic stimuli. Although each LED provides irradiance with relative steep peak, the relative broad bandwidth in our study might reduce the sensitivity to determine the difference depending on the stimulus wavelength. Using shorter, e.g., 400 nm, and longer, e.g., 700 nm, wavelength stimuli might have increased the sensitivity.

In conclusion, our results showed that the SCE can be determined objectively by the FMERGs. They also indicate that the SCE must be considered in interpreting the results of electrophysiological studies, particularly when focal stimuli are used to assess the macular area. Because the SCE is dependent on the passage of light through the outer segments of the photoreceptors, the FMERGs can be used to examine the alignment and integrity of the photoreceptors of the fovea in different types of macular diseases.

Acknowledgments

Support of this study was provided by Researches on Sensory and Communicative Disorders from the Ministry of Health, Labor, and Welfare, Japan. No author has a financial or proprietary interest in any material or method mentioned.

Commercial relationship: none.
Correspondence: Kei Shinoda, M.D., Ph.D.
Email: shinodak@med.teikyo-u.ac.jp.
Address: Department of Ophthalmology, Teikyo University School of Medicine, Kaga 2-11-1, Itabashi-ku, Tokyo 173-8605, Japan.

References

Alpern, M. (1986). The Stiles–Crawford effect of the second kind (SCII): A review. *Perception, 15,* 785–799.

Alpern, M., Kitahara, H., & Fielder, G. H. (1987). The change in color matches with retinal angle of incidence of the colorimeter beams. *Vision Research, 27,* 1763–1778.

Alpern, M., & Kitahara, K. (1983). The directional sensitivities of the Stiles' colour mechanisms. *The Journal of Physiology, 338,* 627–649.

Birch, D. G., Sandberg, M. A., & Berson, E. L. (1982). The Stiles–Crawford effect in retinitis pigmentosa. *Investigative Ophthalmology & Visual Science, 22,* 157–164.

Bush, R. A., & Sieving, P. A. (1994). A proximal retinal component in the primate photopic ERG a-wave. *Investigative Ophthalmology & Visual Science, 35,* 635–645.

Choshi, T., Matsumoto, C. S., & Nakatsuka, K. (2003). Rod-driven focal macular electroretinogram. *Japanese Journal of Ophthalmology, 47,* 356–361.

DeLint, P. J., Berendschot, T. T., & van Norren, D. (1998). A comparison of the optical Stiles–Crawford effect and retinal densitometry in a clinical setting. *Investigative Ophthalmology & Visual Science, 39,* 1519–1523.

DeLint, P. J., Vos, J. J., Berendschot, T. T. & van Norren, D. (1997). On the Stiles–Crawford effect with age. *Investigative Ophthalmology & Visual Science, 38,* 1271–1274.

Gao, W., Cense, B., Zhang, Y., Jonnal, R. S., & Donald, T. M. (2008). Measuring retinal contributions to the optical Stiles–Crawford effect with optical coherence tomography. *Optics Express, 16,* 6486–6501.

Kondo, M., Miyake, Y., Horiguchi, M., Suzuki, S., & Tanikawa, A. (1998). Recording multifocal electroretinogram on and off responses in humans. *Investigative Ophthalmology & Visual Science, 39,* 574–580.

Kurimoto, Y., Kondo, M., Ueno, S., Sakai, T., Machida, S., & Terasaki, H. (2009). Asymmetry of focal macular photopic negative responses (PhNRs) in monkeys. *Experimental Eye Research, 88,* 92–98.

Sieving, P. A., Murayama, K., & Naarendorp, F. (1994). Push–pull model of the primate photopic electroretinogram: A role for hyperpolarizing neurons in shaping the b-wave. *Visual Neuroscience, 11,* 519–532.

Stiles, W. S. (1937). The luminous efficiency of monochromatic rays entering the eye pupil at different points and a new colour effect. *Proceedings of the Royal Society of London B: Biological Sciences, 137,* 90–118.

Stiles, W. S., & Crawford, B. H. (1933). The luminous efficiency of rays entering the eye pupil at different points. *Proceedings of the Royal Society of London B: Biological Sciences, 112,* 428–450.

Yamada, K., Matsumoto, C. S., & Nakatsuka, K. (2006). Effect of spatial frequency of stimulus on focal macular ERGs in monkeys. *Documenta Ophthalmologica, 113,* 83–91.

Yamamoto, S., Gouras, P., & Lopez, R. (1995). The focal cone electroretinogram. *Vision Research, 35,* 1641–1649.

Doc Ophthalmol (2012) 124:91–98
DOI 10.1007/s10633-011-9307-9

ORIGINAL RESEARCH ARTICLE

Macular function evaluated by focal macular electroretinograms after reduced fluence photodynamic therapy in eyes with polypoidal choroidal vasculopathy

Shigeki Machida · Tomoharu Nishimura · Kunifusa Tamada · Tomomi Harada · Daijiro Kurosaka

Received: 19 October 2011 / Accepted: 19 December 2011 / Published online: 31 December 2011

Abstract The purpose of this study was to evaluate the macular function by measuring the focal macular electroretinograms (ERGs) recorded before and after reduced fluence photodynamic therapy (RFPDT) in patients with polypoidal choroidal vasculopathy (PCV). Eleven eyes of 11 patients with PCV were studied. Their ages ranged from 62 to 85 years with a mean of 74.7 ± 6.9 years. The exposure time for the RFPDT was reduced to 42 s, so that the total energy of the laser was approximately one-half that of the standard PDT. We measured the visual acuity, foveal thickness, and focal macular ERGs before and after the RFPDT. The follow-up period ranged from 13 to 34 months with a mean of 26 months after the treatment. A significant recovery of vision was seen even at 1 week after the RFPDT ($P < 0.005$), and the visual acuities improved gradually thereafter ($P < 0.0005$). The foveal thickness was significantly reduced at 1 week after the treatment ($P < 0.005$) and then continued to become significantly thinner with time ($P < 0.0001$). A slight recovery of the a- and b-wave amplitudes was seen postoperatively without a transient reduction in the amplitudes. The b-wave amplitude was significantly larger at 3 months after the treatment than at baseline ($P < 0.05$). Choroidal hypoperfusion did not develop 3 months postoperatively in the indocyanine green angiograms. Exudative changes recurred in 4 (27%) eyes after 1 year and in 9 (82%) eyes during the follow-up period. RFPDT provided short-term benefits in selected patients with PCV with small lesions. The macular function was retained after RFPDT without a transient decrease in visual function. Further study is needed to determine the long-term efficacy of RFPDT for eyes with PCV.

Keywords Photodynamic therapy · Reduced fluence · Electroretinogram (ERG) · Focal ERG · Polypoidal choroidal vasculopathy (PCV)

S. Machida (✉) · T. Nishimura · K. Tamada · T. Harada · D. Kurosaka
Department of Ophthalmology, Iwate Medical University School of Medicine, 19-1 Uchimaru, Morioka, Iwate 020-8505, Japan
e-mail: smachida@iwate-med.ac.jp

Introduction

Polypoidal choroidal vasculopathy (PCV) is characterized by an abnormal choroidal vascular network with polypoidal dilatations of the choroidal vessels [1, 2]. PCV is the most prevalent subtype of age-related macular degeneration (AMD) in Japan and other Asian countries [3–5].

Photodynamic therapy (PDT) has been shown to have therapeutic benefit in patients with PCV especially in Japan [6, 7]. PDT is highly recommended in cases with smaller lesions, and good visual outcomes have been obtained after PDT [8].

One of the unfavorable side effects of PDT is a dysfunction of the macula associated with

hypoperfusion of the choroids [9]. Ishikawa et al. [10] evaluated the macular function by the focal macular electroretinograms (ERGs) after PDT in patients with AMD including those with PCV. The focal macular ERGs were decreased at 1 week and 1 month after PDT. However, the focal responses recovered to the baseline level after 3 months. They showed a significant correlation between the decrease in the focal macular ERGs and choroidal hypoperfusion that developed after PDT. Lai et al. also demonstrated a transient reduction in the amplitudes of the multifocal ERGs after PDT [11].

Michells et al. reported on the use of reduced fluence PDT (RFPDT) in which the irradiation energy or exposure time was reduced to one-half of the standard energy for PDT [12]. They reported that RFPDT closed choroidal neovascularization (CNV) in patients with age-related macular degeneration (AMD) without appearing to disturb the choroidal circulation. Yamashita et al. [13] treated patients with PCV by RFPDT and reported good anatomical and visual outcomes after 1 year with an average of 1.3 treatments/year.

The purpose of this study was to evaluate the macular function following RFPDT in Japanese patients with PCV by measuring the focal macular ERGs.

Methods

Subjects

Eleven eyes of 11 patients (9 men and 2 women) with PCV were studied. The patients were treated in the Retinal Unit of the Iwate Medical University Hospital, and their ages ranged from 62 to 85 years with a mean of 74.7 ± 6.9 years. The clinical characteristics of all patients are shown in Table 1. All patients received comprehensive ophthalmological examinations including measurement of the Snellen visual acuity, indirect ophthalmoscopy, and slit-lamp examination at every visit. In addition, color fundus photographs, fluorescein angiography (FAG), indocyanine green angiography (ICGA), and optical coherence tomography (OCT) were recorded. The foveal thickness was measured from the inner limiting membrane (ILM) to outer border of the RPE. When a retinal pigment epithelial detachment was present, we measured from the ILM to Bruch's membrane instead of the RPE. The follow-up periods ranged from 13 to 34 months with a mean of 26 ± 6.7 months.

The diagnosis of PCV was made based on the diagnostic criterion proposed by the Japanese research group of PCV [14]. Patients with subretinal elevated orange lesions or polypoidal structures in the ICGA images were defined as having PCV. The greatest linear dimension (GLD) of the polypoidal structures and vascular network was measured in all eyes. We included patients with unilateral PCV whose GLD of the vascular lesions was less than 4,000 μm but more than 2,000 μm. So most of the treated area overlapped the retinal area from which the focal macular ERGs were elicited (Fig. 1d). The GLD ranged from 2,340 to 3,975 μm with a mean of 2,886 ± 528 μm.

This research was conducted in accordance with the Institutional Guidelines of the Iwate Medical

Table 1 Characteristics of patients

Age	Gender	GLD	BCVA (logMAR)		Foveal thickness (μm)		Follow-up (months)
			Baseline	3 months	Baseline	3 months	
62	M	3,113	0.60	0.60	413	301	34
65	M	2,744	0.70	0.30	360	185	30
70	M	3,975	1.00	0.80	266	191	25
74	F	3,479	0.90	0.30	454	256	26
75	M	2,340	0.30	0.16	287	178	20
76	M	2,653	0.80	0.70	443	287	30
76	F	2,459	0.60	0.40	454	252	29
78	M	2,588	0.16	0.20	447	347	13
79	M	3,375	0.90	0.90	575	307	30
82	M	2,396	0.16	0.10	283	239	18
85	M	2,620	0.60	0.30	400	290	34

GLD greatest linear dimension, *BCVA* best-corrected visual acuity, *MAR* minimum angle of resolution, *M* male, *F* female

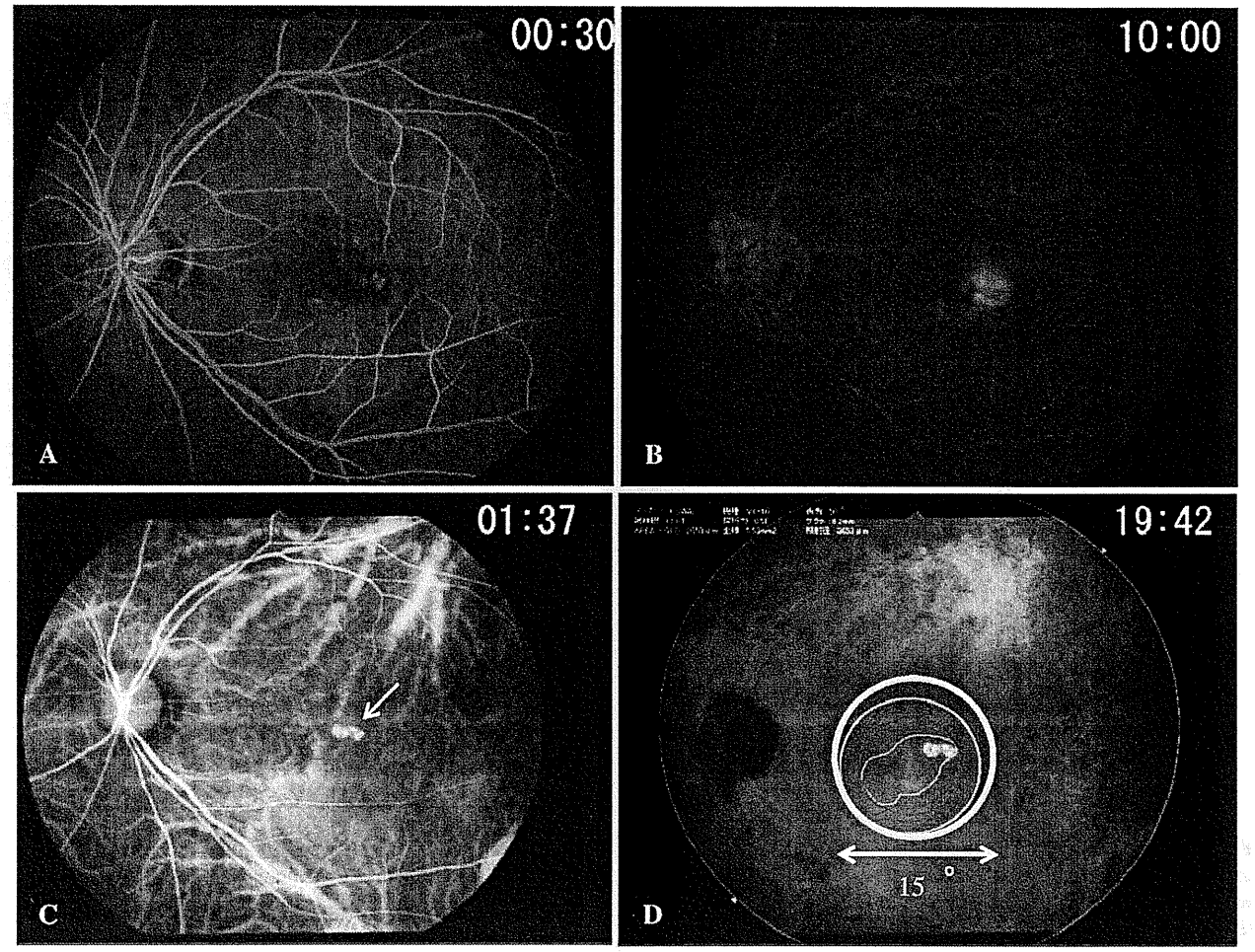

Fig. 1 Representative case of polypoidal choroidal vasculopathy. Early-phase fluorescein angiogram is shown in **a** and late phase in **b**. Indocyanine green angiograms at the early phase are shown in **c** and late phase in **d**. The *pink circle* has a diameter of the greatest linear dimension of the lesion (**d**). The *blue circle* represents the area treated by reduced fluence photodynamic therapy. The *white circle* represents the retinal area from which the focal macular electroretinograms were elicited

University, and the procedures conformed to the tenets of the Declaration of Helsinki. An informed consent was obtained from all subjects after a full explanation of the nature of the experiments.

Reduced fluence photodynamic therapy (RFPDT)

We performed a single RFPDT with veteporfin (Visdyne®) on all patients using standard parameters except for the exposure time. Briefly, the patients were given 6 mg of Visdyne®/meter^2 of body surface area in 5% glucose dilution intravenously over a period of 10 min. Fifteen minutes after the start of the infusion, the fundus was irradiated with a 689-nm diode laser at an intensity of 600 mW. The exposure time was reduced to 42 s, so that the total energy of the laser was approximately 25 J/cm^2 [12]. After the treatment, the patients were instructed to avoid sunlight and to wear sunglasses for 5 days.

Focal macular ERGs

Before the ERG recordings, the pupils were confirmed to be maximally dilated to approximately 8 mm diameter following a topical application of a mixture of 0.5% tropicamide and 0.5% phenylephrine HCL. The stimulus and observation system was integrated into an infrared fundus camera (Mayo Co., Nagoya, Japan). This system for recording focal macular ERGs under direct observation was developed by Miyake

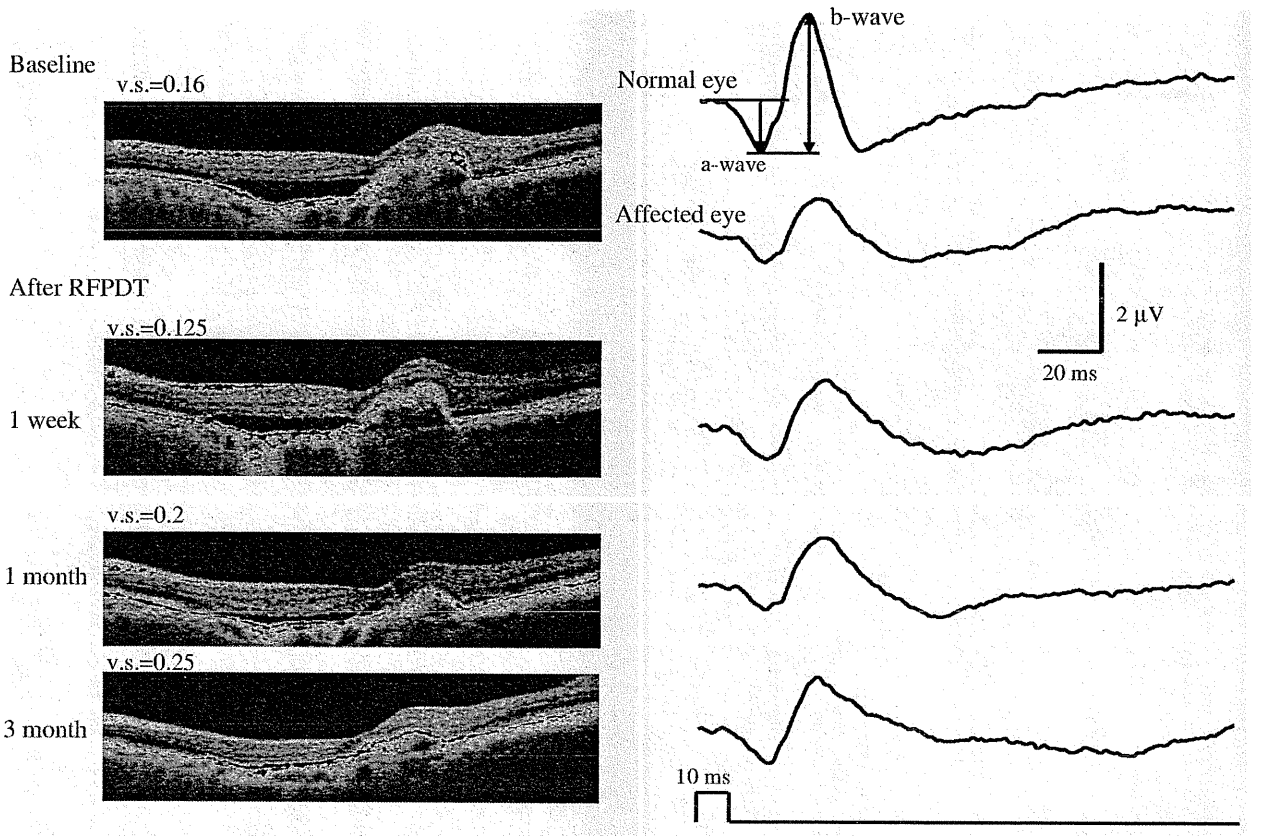

Fig. 2 Optical coherence tomographic (OCT) images and focal macular electroretinograms (ERGs) of a representative case with polypoidal choroidal vasculopathy before the treatment (*baseline*) and after reduced fluence photodynamic therapy (RFPDT). The OCT images were obtained by horizontal scans through the macula. Note that there was no reduction in the amplitudes of the focal macular ERGs after RFPDT

et al. [15]. The stimulus spot was 15 degrees in diameter and was placed on the macular area. During the ERG recordings, the stimulus spot was monitored so that it remained on the macular area. The white stimulus and background lights were generated by light-emitting diodes (LEDs) that had maximal spectral emissions at 440–460 nm and 550–580 nm. The intensity of the stimulus was 165 cd/m^2 and that of the background light was 6.9 cd/m^2. The stimulus duration was 10 ms.

After the cornea was anesthetized with 4% lidocaine HCL and 0.4% oxybuprocaine HCL, a Burian-Allen bipolar contact lens electrode (Hansen Ophthalmic Laboratories, Iowa City, IA) was inserted into the conjunctival sac. A chlorided silver electrode was placed on the left ear lobe as the ground electrode. The responses were digitally band pass filtered from 5 to 500 Hz (Neuropack μ, MEB 9102, Nihonkoden, Tokyo, Japan). Two to three hundred responses were averaged at a stimulation rate of 5 Hz.

The a-wave amplitudes were measured from the baseline to the trough of the first negative wave, and the b-wave amplitudes from the first trough to the peak of the following positive wave. The amplitudes and implicit times were measured for each wave (Fig. 2).

Statistic analysis

The significance of the differences was determined by the Student's two-tailed t tests for paired data. Repeated measures ANOVA was used to determine the statistical significance of the functional and anatomical changes with time after RFPDT. In addition, Tukey's multiple comparison tests were performed after the repeated measures ANOVA as post hoc tests. Statistical significance was set at

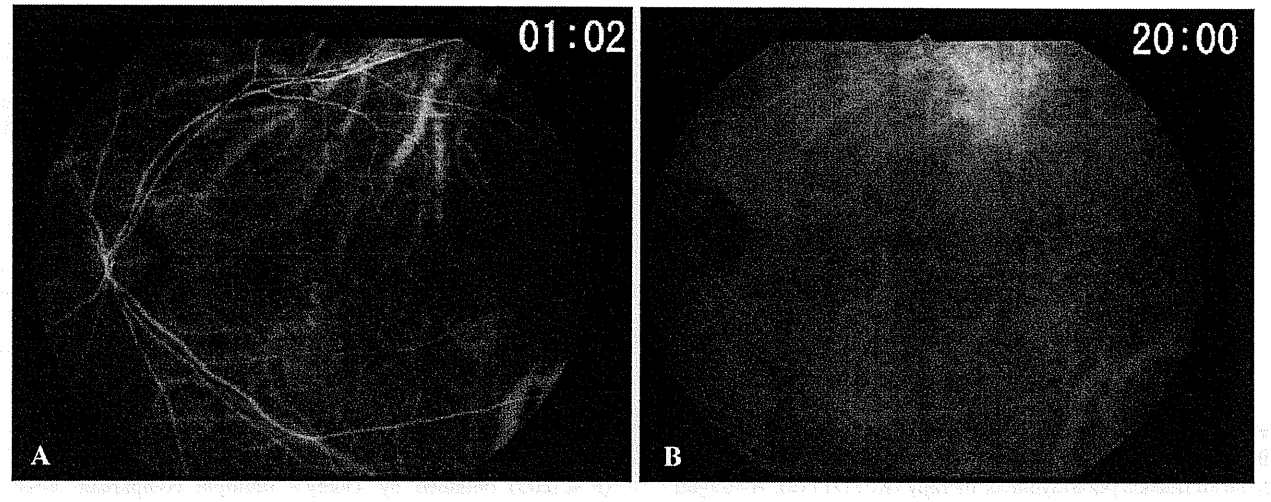

Fig. 3 Indocyanine green angiograms of a representative case with polypoidal choroidal vasculopathy 3 months after reduced fluence photodynamic therapy (RFPDT) are shown. Choroidal hypoperfusion did not develop at either the early (**a**) or late phase (**b**) after RFPDT

$P < 0.05$. All of these analyses were performed with the Prism 5.1 (GraphPad Software Inc., San Diego, CA, USA).

Results

Representative case

The FAG findings in a representative case of PCV with a window defect and dye leakage are shown in Fig. 1a and b. The early phase of ICGA shows the polypoidal structures (Fig. 1c, arrows), and the dye leakage and staining at the late stage (Fig. 1d) suggesting the existence of an abnormal vascular network. The GLD of the polypoidal structures and staining area was 2,750 μm. RFPDT was applied with a spot size of 3,750 μm diameter which is marked by the blue line in Fig. 1d.

At the baseline, a pigment epithelial detachment (PED) with serous retinal detachment (SRD) involving the fovea was seen in the OCT image (Fig. 2). Although there was no difference in the size and height of the PED and SRD 1 week after the RFPDR, these lesions gradually decreased with time accompanied by a recovery of the visual acuity. Representative focal macular ERGs recorded from the affected eye and normal fellow eye are shown in the right column of Fig. 2. At the baseline, the amplitudes of the a- and b-waves were smaller with longer implicit times in the affected eye than that of the normal fellow eye. There was no reduction in the amplitudes of these waves at any time points after the treatment. The ERG responses appeared to be larger at 3 months postoperatively than at the baseline.

A hypofluorescent area representing choroidal hypoperfusion was not seen in the early and late phases of ICGA recorded 3 months after the treatment (Fig. 3a, b).

Changes in visual acuity and foveal thickness after RFPDT

The best-corrected visual acuities in logarithm of the minimum angle of resolution (logMAR) units obtained from each patient at the baseline, 1 week, and 1, 2 and 3 months following RFPDT are plotted in Fig. 4a. A significant recovery of the visual acuities was seen as early as 1 week after RFPDT (t test: $P < 0.005$), and the visual acuities improved gradually with increasing postoperative time (repeated measures ANOVA: $P < 0.005$). Significant differences were found after RFPDT at all time points from the baseline visual acuity (Tukey's multiple comparison test, $P < 0.05$). The foveal thickness is plotted for each patient at the baseline, 1 week, and 1 and 3 months following RFPDT in Fig. 4b. The foveal thickness was significantly reduced at 1 week after the RFPDT (t test: $P < 0.005$), and the fovea continued to become thinner with time (repeated measures

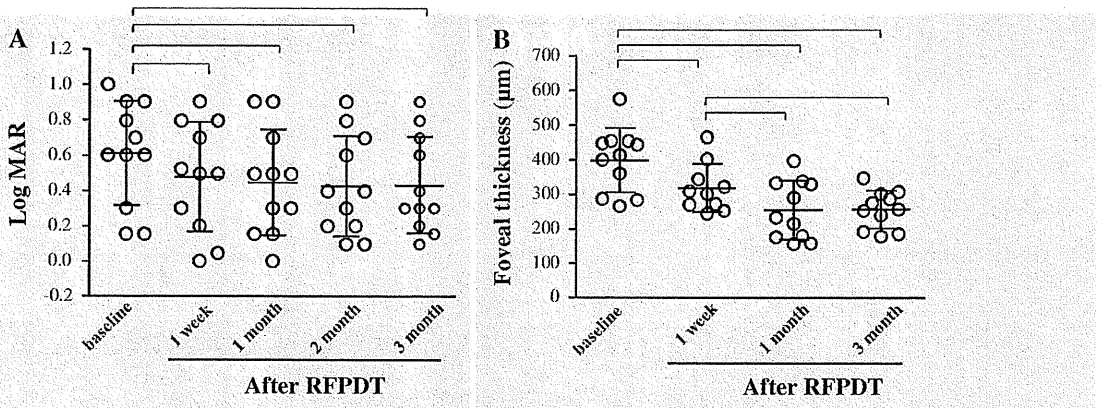

Fig. 4 Averaged best-corrected visual acuity in logarithm of the minimum angle resolution (logMAR) units before and after reduced fluence photodynamic therapy (RFPDT) (**a**). Averaged foveal thickness measured by optic coherence tomography before and after RFPDT (**b**). *Error bars*: mean ± standard deviation. *Hooked lines* represent statistical significance ($P < 0.05$) obtained by Tukey's multiple comparison after repeated measure ANOVA

ANOVA: $P < 0.0001$). Multiple comparison demonstrated that there were significant differences ($P < 0.05$) between each time point except between 1 and 3 months after RFPDT.

Changes in focal macular ERGs after RFPDT

The amplitudes of the a- and b-waves were significantly reduced, and the implicit times were prolonged at the baseline compared to the unaffected normal fellow eyes (Figs. 5 and 6). The a- and b-wave amplitudes did not change significantly after the treatment. A slight recovery of the a-wave amplitudes was seen postoperatively although the increase was not significant (Fig. 5a). The b-waves also had a slight recovery in the amplitude but the change was not significant; however, at 3 months after the treatment, the b-wave amplitude was significantly larger than that at the baseline (Fig. 5b, *t* test: $P < 0.05$).

The implicit times of the a- and b-waves were significantly prolonged in the diseased eyes compared to the unaffected normal fellow eyes (Fig. 6a, b). No recovery of the implicit times was seen for the a- and b-waves postoperatively. A significant reduction in the amplitude and increase in the implicit time were not seen at any time point after the treatment.

Complications and recurrences of exudative changes

A closure of the polypoidal structures was observed by ICGA in 8 eyes (73%) at 3 months after the RFPDT.

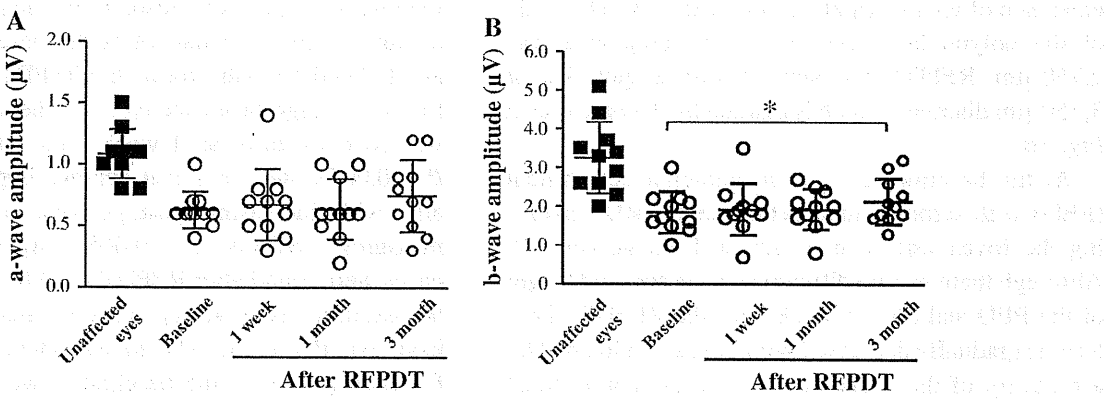

Fig. 5 Averaged amplitudes of the focal macular electroretinograms (ERG) a- (**a**) and b-waves (**b**). *Circles* represent the eyes affected by polypoidal choroidal vasculopathy before and after reduced fluence photodynamic therapy (RFPDT). *Filled squares* represent unaffected eyes of the patients. *Error bars*: mean ± standard deviation. *Asterisk* represents significant difference compared to the baseline (*t* test, $P < 0.05$)